These results indicate that there is only one form of CN^- present in the polymerized derivative and that a majority of the cyanide ligands are bridging in nature. Both the oxidation state of the Fe moiety and the fact that the surface complex contains mainly bridging $\nu(CN)$ add further support for the assignment of this species as the $[Fe^{II}Pt^{IV}]_n$ polymer. The presence of Pt(IV) on the surface is confirmed by analogy to other ammineplatinum compounds as shown in Table I. The ammine assignments are likewise very similar to those reported for Ni_2I on the Ni surface, all corresponding to the Pt(IV) oxidation state.

Cyclic voltammograms of the electropolymerized species on SnO_2 (using derivatization times of less than 30 s) show two quasireversible redox waves (see Figure 11) in 1 M $NaNO_3$, occurring at 0.86 and 1.09 V vs SCE. These peaks are not cation dependent. As in the case of the nickel complex, no X-ray powder diffraction peaks are observed that can be attributed to the polymer. Thus, it appears that the polymerized surface species does not form a crystalline lattice. If longer derivatization times are employed, only one cyclic voltammetric peak is observed prior to the anodic solvent window cutoff. The exact reasons for these dissimilar results are the subject of continued study.[12]

The above results merit a reevaluation of the electrochemistry of Ni_2I on a Ni surface since the cyclic voltammetric peaks of this complex might also be explained in terms of electropolymerization of $[Pt(NH_3)_4]_2I$ on Ni. However, control experiments utilizing a nickel working electrode with the K^+-exchanged complex K_4I demonstrated that an interfacial layer is still formed on the Ni surface. This interface yielded a cyclic voltammogram in 1 M $NaNO_3$ which was identical with that obtained for Ni_2I on Ni. In addition, a comparison of the UV-vis spectroscopy of the Ni_2I on nickel-plated SnO_2 vs the polymerized complex shows a shift in the IT band from 416 to 570 nm. Therefore, one can conclude that the reported chemistry of $[Pt(NH_3)_4]_2I$ at a Ni surface is distinctly different from that at SnO_2 or Pt. In the former case, $[Pt(NH_3)_4]_2I$ preferentially forms a Ni(II) precipitate, whereas electropolymerization occurs at the latter electrodes.

The following mechanism is postulated for the formation of the polymerized interfacial structure. Oxidation of "$[Fe^{II}Pt^{IV}Fe^{II}]^{4-}$" at a potential of 1.4 V vs SCE generates "$[Fe^{III}Pt^{IV}Fe^{III}]^{2-}$." This species can then oxidize one of the $Pt(NH_3)_4^{2+}$ counterions to form the polymeric chain "$[Fe^{II}Pt^{IV}]_n$" as depicted below. Reoxidation of "$[Fe^{II}Pt^{IV}]_n$" allows for further chain growth:

$$n\mathrm{Fe^{II}Pt^{IV}Fe^{II}} \rightarrow n\mathrm{Fe^{III}Pt^{IV}Fe^{III}} + 2ne^- \quad (1)$$

$$n\mathrm{Fe^{III}Pt^{IV}Fe^{III}} + n\mathrm{Pt^{II}} \rightarrow [\mathrm{Fe^{II}Pt^{IV}}]_{2n} \quad (2)$$

$$[\mathrm{Fe^{II}Pt^{IV}}]_{2n} \rightarrow [\mathrm{Fe^{III}Pt^{IV}}]_{2n} + 2ne^- \quad (3)$$

$$[\mathrm{Fe^{III}Pt^{IV}}]_{2n} + \mathrm{Pt^{II}} \rightarrow [\mathrm{Fe^{II}Pt^{IV}}]_{2n+1} \quad (4)$$

Acknowledgment. This work was supported by the National Science Foundation under Grant No. CHE-8700868. We thank M. Zhou and J. L. Steiger for technical assistance and valuable discussions.

(12) While a shift in redox potential with organic polymer chain length is not to be expected, the coordination chemistry of the described inorganic "polymer" dictates that such a relationship should exist. Specifically, in the present case, polymer chain and/or degree of branching is related to the number of terminal versus bridging cyanide ligands. It has previously been reported[13] that the redox potential of cyanometalate complexes is strongly dependent on the environment of the cyanide nitrogen lone pair. Thus, even moderate changes in the solvent environment can have a dramatic effect on redox potential.[14] Therefore, the observed redox potential for the polymer should be a strong function of the ratio of terminal cyanides to cyanides in which the nitrogen forms a dative bond.

(13) Gutmann, V.; Gritzner, G.; Danksagmüller, K. *Inorg. Chim. Acta* **1976** *17*, 81.

(14) Gritzner, G.; Danksagmüller, K.; Gutmann, V. *J. Electroanal. Chem. Interfacial Electrochem.* **1976**, *72*, 177.

Contribution from the Chemistry and Physics Laboratory, The Aerospace Corporation, El Segundo, California 90245, and Department of Physics, University of California, Riverside, California 92521

Photoelectron Spectroscopic Studies of the Electronic Structure of α-SiC

Stephen V. Didziulis,*,† Jeffrey R. Lince,† Paul D. Fleischauer,† and Jory A. Yarmoff‡

Received April 4, 1990

The electronic structure of single-crystal α-SiC (silicon carbide) has been determined with variable photon energy valence band photoelectron spectroscopy. Synchrotron radiation in the range 30–250 eV was used in addition to a conventional Al Kα X-ray source to follow the intensity changes of valence band features as a function of the incident photon energy. The dominant atomic orbital contributions have been assigned to valence band features by comparing them to theoretical atomic photoionization cross sections. The results indicate that C 2s based ionizations appear at the highest binding energy, near 15 eV, while Si 3s features are evident near 10 eV. The highest occupied energy levels (from approximately 1–8-eV binding energies) are predominantly C 2p based. Differences between the photon energy dependence of the data and theoretical atomic orbital cross sections show the valence levels to be highly mixed. Comparison of the valence band spectra with a molecular orbital calculation confirms the experimental assignments, but the calculation appears to underestimate the extent of atomic orbital mixing. The valence band spectrum of a hot-pressed polycrystalline SiC sample compares quite well with the single-crystal spectrum. The implications of these results on the chemisorption behavior and reactivity of SiC are discussed.

Introduction

Silicon carbide (SiC) has attracted interest for electronic applications as a possible hostile environment semiconductor and for tribological applications as an abrasive and as a candidate for wear-resistant mechanical parts. SiC is an excellent candidate for all these applications because of its high hardness, high melting point, and relative chemical inertness. Despite the interest shown in SiC, little experimental work has been performed to determine its electronic structure.[1-5] The work presented in this paper uses variable photon energy valence band photoelectron spectroscopy (PES) to study the electronic structure of α-SiC.

Electronic structure is of obvious importance in electronic applications, which require high-purity materials for device production. In this regard, SiC poses a problem, however, because it grows in a variety of crystal structures. The wurtzite (or α) phase is easiest to grow but exists in over 100 different polytypes, which actually consist of mixtures of hexagonal and cubic packing.

†The Aerospace Corp.
‡University of California.

(1) Hoechst, H.; Tang, M.; Johnson, B. C.; Meese, J. M.; Zajac, G. W.; Fleisch, T. H. *J. Vac. Sci. Technol., A* **1987**, *5*, 1640.
(2) Sasaki, T. A.; Baba, Y. JAERI-M Report 85-063; Japan Atomic Energy Research Institute: Tokai-Mura, Japan, 1985.
(3) Xu, X.; Zhang, F.; Chen, G. *J. Non-Cryst. Solids* **1987**, *90*, 295.
(4) Parrill, T. M.; Bermudez, V. M. *Solid State Commun.* **1987**, *63*, 231.
(5) Fang, R.-C.; Ley, L. *Phys. Rev. B* **1989**, *40*, 3818.

0020-1669/91/1330-0672$02.50/0

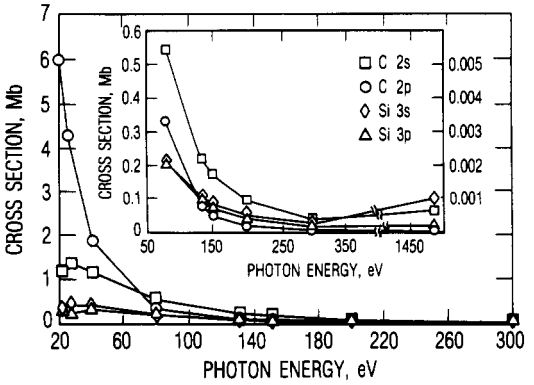

Figure 1. Theoretical atomic photoionization cross sections for the important valence levels in SiC. The inset gives an expanded view of the 80–1486.6-eV values. (Adapted from ref 16.)

The different polytypes have band gaps varying from 2.5 to 3.2 eV. Purely hexagonal SiC (2H) is virtually impossible to grow as a single polytype, single crystal because of low stacking fault energies.[6] The zinc blende (or β) phase has a well-defined band gap of 2.2 eV but has proven quite difficult to grow by conventional crystal growth techniques. However, recent advances in chemical vapor deposition have resulted in the production of thin films of single-crystal β-SiC.[1,7-9]

Electronic structure is also of importance in the surface chemistry of materials, which, in turn, affects many tribological properties. The density of states in the valence band plays a major role in both bonding to and reaction of materials, key factors in the lubrication and wear of SiC. These tribological properties should be well understood to define the utility of SiC in mechanical applications. Unlike electronic applications, tribological applications are not limited by the need for single-phase materials, making SiC potentially more useful. However, single crystals are certainly preferred in valence band PES, and single-crystal α-SiC samples are used in this study.

Valence band PES has been used to examine SiC surface chemistry in several studies. In general, this technique has been used diagnostically to determine if a chemical reaction has occurred between SiC and deposited metal films.[10-13] One of these studies[10] makes an important comparison of the X-ray photoelectron spectroscopy (XPS) valence band spectra of silicon, diamond, and SiC. The valence bands of the three tetrahedrally bonded materials have somewhat similar shapes, but relative peak intensities and energy splittings are significantly different. Valence band PES data have also been collected on single-crystal α-SiC at selected photon energies to compare to β-SiC films, reconstructed surfaces, and substoichiometric SiC phases and to distinguish bulk and surface contributions to the spectra.[4,5] In addition, a recent study[1] examined the valence band of β-SiC films with variable photon energy angle-resolved PES. Synchrotron radiation was used in the energy range 14–24 eV to determine the dispersion of valence band features, which compare favorably with theoretical band structure calculations.[14,15]

The present work uses variable photon energy angle-integrated PES over a much broader energy range than the study just mentioned. In particular, the valence band of a clean single-crystal α-SiC sample is obtained with synchrotron radiation from 30 to 250 eV and with a conventional X-ray anode at 1486.6 eV. The changes in relative intensities of valence band features with photon energy are used to assign the dominant atomic character in valence band peaks through comparison to theoretical atomic photoionization cross sections. This type of analysis is particularly difficult for highly covalent materials because of the extensive mixing of atomic levels in valence band states. For this study, a photon energy range is required where cross sections of the atomic constituents vary in significantly different ways. Figure 1 exhibits the theoretical atomic photoionization cross sections for the valence levels of Si and C as a function of photon energy.[16] The C 2s and C 2p photoionization cross sections drop dramatically relative to Si features in the photon energy range 30–250 eV, the primary range used in this work. The inset of Figure 1 shows these changes from 80 to 1486.6 eV in more detail. The experimental PES peak assignments are then compared to theoretical electronic structure calculations.[17] Finally, the XPS valence band of a polycrystalline SiC sample is compared to the single-crystal SiC results.

Experimental Section

Single crystals of α-SiC were obtained from Atomergic Chemicals Corp., Plainview, NY. These hexagonal crystals had one smooth side and a very rough face, which have been identified in the literature as the (000$\bar{1}$) and (0001) surfaces, respectively.[18] The (000$\bar{1}$) surface was used in this work. The samples were aligned along the c axis with Laue back-diffraction and then polished on both sides with successively smaller grit diamond paste down to 0.25 μm. The crystals were etched in a buffered HF solution and rinsed in methanol to remove any thick oxide layer. Further cleaning was performed in ultrahigh vacuum (UHV) with argon ion sputter/anneal cycles. Samples were sputtered at 1 kV for 5 min, followed by sputtering at 500 and 300 V each for 15 min while being heated at 550 °C.[19] Sputtering at 1 kV was needed to remove any remaining oxide layer and surface contaminants, while the lower energy bombardment and high temperature prevented the implantation of argon ions.

Valence band photoelectron spectra were obtained with synchrotron radiation from beam line UV-8B at the National Synchrotron Light Source (NSLS). The beam line is described in detail elsewhere.[20] Photons in the 30–70-eV energy range were obtained with the 822 groove/mm grating on the 6-m monochromator, 100–130-eV data were obtained with the 288 groove/mm grating on the 6-m monochromator, and 150–250-eV photons were obtained with the 1800 groove/mm grating on the 10-m monochromator. The electron spectrometer was a high-resolution ellipsoidal mirror display analyzer with a 1.8-sr angular acceptance.[21] The energy resolution of the system (including both the analyzer and the monochromator) was estimated to be 0.3–0.5 eV in the photon energy range used. The ion-pumped vacuum system was composed of the analyzer chamber and a sample preparation chamber, separated by a gate valve. Each chamber had a base pressure in the low 10^{-10}-Torr regime. Sputter/anneal cycles were performed in the sample preparation chamber with a Perkin-Elmer Physical Electronics ion gun in 5×10^{-5} Torr of Ar, and sample annealing was performed by direct resistive heating. Cycles were repeated until only SiC features were observed in the valence band (vide infra). The spectra obtained were normalized to the incident photon flux by monitoring the photoelectric current on the gold-coated beam line refocusing mirror near the entrance to the analyzer chamber.

Prior to obtaining the synchrotron data, XPS was performed on the samples at The Aerospace Corp. with a Surface Science Instruments (SSI) SSX-100 small-spot XPS instrument to determine the optimum sample cleaning procedures. This instrument uses monochromatized Al Kα radiation and a high-throughput spherical sector electron energy analyzer. The ion-pumped vacuum system housing the SSI instrument had a base pressure of better than 1×10^{-10} Torr. This system also contained a differentially pumped Leybold-Heraeus IQE 12/38 ion gun and a tungsten filament for sample heating, located behind the sample

(6) Evans, P. E., Eng, C., Dobson, M. M., Eds. *Silicon Carbide Alloys, Research Reports in Materials Science*, series 1; Parthenon Press: 1986.
(7) Suzuki, A.; Furukawa, K.; Higashigaki, Y.; Harada, S.; Nakajima, S.; Inoguchi, T. *J. Cryst. Growth* **1984**, *70*, 287.
(8) Addamiano, A.; Klein, P. H. *J. Cryst. Growth* **1984**, *70*, 291.
(9) Liaw, P.; Davis, R. F. *J. Electrochem. Soc.* **1985**, *132*, 642.
(10) Porte, L. *J. Appl. Phys.* **1986**, *60*, 635.
(11) Hoechst, H.; Niles, D. W.; Zajac, G. W.; Fleisch, T. H.; Johnson, B. C.; Meese, J. M. *J. Vac. Sci. Technol., B* **1988**, *6*, 1320.
(12) Niles, D. W.; Hoechst, H.; Zajac, G. W.; Fleisch, T. H.; Johnson, B. C.; Meese, J. M. *J. Vac. Sci. Technol., A* **1988**, *6*, 1584.
(13) Niles, D. W.; Hoechst, H.; Zajac, G. W.; Fleisch, T. H.; Johnson, B. C.; Meese, J. M. *J. Appl. Phys.* **1989**, *65*, 662.
(14) Lubinsky, A. R.; Ellis, D. E.; Painter, G. S. *Phys. Rev. B.* **1975**, *11*, 1537.
(15) Li, Y.; Lin-Chung, P. J. *Phys. Rev. B.* **1987**, *36*, 1130.
(16) Yeh, J. J.; Lindau, I. *At. Data Nucl. Data Tables* **1985**, *32*, 1.
(17) Soga, T.; Sasaki, T. A. JAERI-M Report 9769; Japan Atomic Energy Research Institute: Tokai-Mura, Japan, 1981.
(18) Muehlhoff, L.; Choyke, W. J.; Bozack, M. J.; Yates, J. T., Jr. *J. Appl. Phys.* **1986**, *60*, 2842.
(19) Surface graphitization through the loss of Si is known to occur at temperatures greater than 900 K.[18]
(20) Himpsel, F. J.; Jugnet, Y.; Eastman, D. E.; Donelon, J. J.; Grimm, D.; Landgren, G.; Marx, A.; Morar, J. F.; Oden, C.; Pollak, R. A. *Nucl. Instrum. Methods* **1984**, *222*, 107.
(21) Eastman, D. E.; Donelon, J. J.; Hien, N. C.; Himpsel, F. J. *Nucl. Instrum. Methods* **1980**, *172*, 327.

stage. A reverse-view, low-energy electron diffraction (LEED) system, Princeton Research Instruments Model RVL-8-120, was available in a peripheral, although connected, sample preparation chamber.

Approximately 20 sputter/anneal cycles were needed to remove the bulk oxygen. Once this oxygen was removed, a clean, oxygen-free surface could normally be obtained with one or two sputter/anneal cycles. Surfaces were determined to be clean when no O 1s signal was present and the Si 2p level showed a single chemical component with Si $2p_{3/2}$ and $2p_{1/2}$ binding energies of 100.7 and 101.3 eV, respectively.[22] The C 1s level at 283.1 eV was also followed as a function of sample treatment. However, a higher binding energy shoulder near 284.4 eV, whose intensity seemed to scale with the O 1s peak intensity, could not be completely removed from the carbide peak. Samples treated in this fashion exhibited a diffuse 1 × 1 hexagonal LEED pattern. The presence of the LEED pattern indicates that any disorder induced by the Ar ion sputtering is confined to the near surface region. The effects of surface damage on the valence band data should be small and limited to the most surface-sensitive spectra. Valence band XPS data were obtained by signal-averaging many scans (approximately 50–75 for sufficient signal/noise ratios) with a 300-μm spot size and 50-eV analyzer pass energy, parameters that yield a gold $4f_{7/2}$ peak with a full width at half-maximum (FWHM) of 0.9 eV. All binding energies are given relative to the spectrometer Fermi level with the gold $4f_{7/2}$ peak at 84.0 eV.

Additional valence band XPS data were obtained on a polycrystalline hot-pressed (HP) SiC sample containing 0.5% Al_2O_3 as a binder, manufactured by ESK Ceramics. Cleaning procedures for the polycrystalline sample included polishing and UHV sputter/anneal cycles, although an oxygen-free surface was never attained, probably because of the alumina binder. The best prepared surface contained approximately 2 atom % oxygen, as determined by core level XPS, and had only one Si species present. Data were obtained at 1486.6 eV, as described for the single-crystal sample.

Results and Analysis

Cross-Section Intensity Analysis. The valence band PES data obtained from the α-SiC samples over the photon energy range 30–1486.6 eV are presented in Figure 2. Each spectrum in the figure is normalized to its most intense feature to allow comparison of relative intensities with changing photon energy. The general valence band shapes are consistent with previously published spectra at selected photon energies.[1-5] Note that the absolute spectral intensities decrease substantially with increasing photon energy, e.g., by a factor of 3 between 30 and 70 eV.[23] The overall decrease in intensity is predicted from the theoretical atomic photoionization cross sections of the important valence levels in SiC: the C 2s and C 2p levels and the Si 3s and Si 3p levels (Figure 1).

As indicated in Figure 1, the atomic cross sections of the important valence levels decrease in significantly different ways with increasing photon energy. Specifically, the C 2s and particularly the C 2p level ionizations should produce the more intense features at low photon energies. These cross sections then decline much more rapidly than do the Si 3s and Si 3p cross sections as the photon energy is increased. The C 2p cross section exhibits the steepest decline, dropping by a factor of 100 between 40 and 200 eV. At the highest photon energy, 1486.6 eV, the C 2s and Si 3s cross sections are clearly larger than the C 2p and Si 3p cross sections, which would cause the PES peaks arising from the s levels to dominate the XPS valence band.

A qualitative comparison of the atomic cross sections to the data in Figure 2 reveals important insights into peak assignments. There are at least five discernible peaks present in the spectra: an assymetric feature near 15-eV binding energy, containing peaks 1 and 2; peak 3 at approximately 10 eV; peaks 4 and 5 located near 7 and 5 eV, respectively. The features seen near 25-eV binding energy likely result from impurity core levels having large photoionization cross sections. The O 2s, Ar 3s, and Ta 4f (used as the sample holder) ionizations all appear near this binding

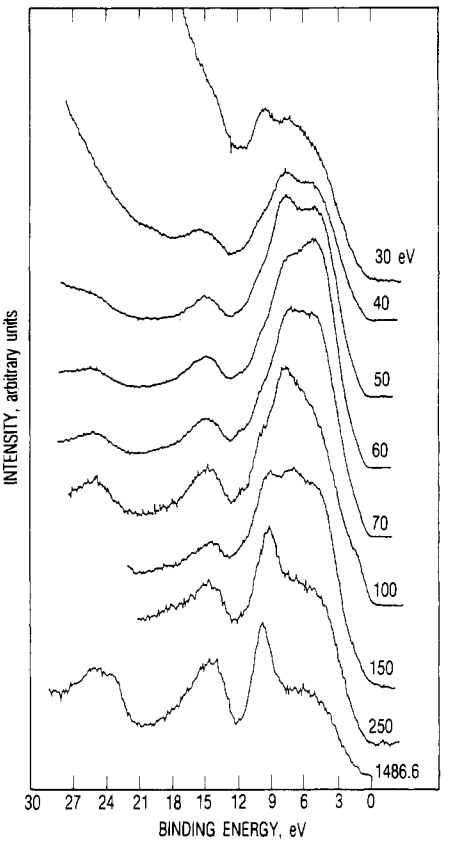

Figure 2. Variable photon energy valence band photoelectron spectra of (000$\bar{1}$) α-SiC obtained at the photon energies listed.

energy. Despite the apparent cleanliness of the sample, these features could be evident from small amounts of these materials.

It is clear from the data that peaks 1–3 increase in intensity relative to the low-binding-energy features with increasing photon energy and dominate the spectrum at 1486.6 eV. This behavior leads to the assignment of peaks 1–3 as ionization from predominantly s-based levels (C 2s–Si 3s) and peaks 4 and 5 (the low binding energy photoemission features) as ionization from dominantly p-based energy levels. In addition, the low-binding-energy peaks 4 and 5 are the more intense features at low photon energy and drop precipitously in the 100–250-eV photon energy region.[24] The intensity changes of peaks 4 and 5 are very important, because the theoretical cross sections in Figure 1 indicate that the C 2p level should have this dramatic decrease relative to all other atomic components. In comparison, the Si 3p levels would actually increase in intensity relative to the C 2s level and have only a very small drop relative to the Si 3s level. This intensity behavior clearly identifies the low binding energy features of the valence band as being dominantly C 2p based ionizations. These assignments are consistent with the ordering of atomic ionization energies where the C 2s level would have the largest ionization energy, followed by the Si 3s, C 2p, and Si 3p levels. It is assumed throughout this paper that changes in the photoionization cross sections dominate the measured PES intensity changes. Therefore, this discussion implicitly assumes that the bulk and surface spectral contributions are similar despite the small and changing sampling depths over the photon energy range used. The lack of any observable surface state in the band gap indicates that no drastic differences in surface PES contributions exist; however, we cannot rule out effects occurring due to some surface reconstruction.

The spectral intensity changes were further investigated by fitting the valence band with six Gaussian–Lorentzian peaks (Voigt functions), as indicated for the 50-eV spectrum in Figure 3. The best fits were obtained with functions having 90–95% Gaussian

(22) The Si 2p spin–orbit splitting was not resolved by XPS. The $2p_{3/2}$ and $2p_{1/2}$ binding energies were determined by a two-peak fit of the data with a constrained 0.6-eV splitting using the SSI peak-fitting program.

(23) It proved impossible to compare the absolute intensities for data obtained with different gratings and monochromators, but the intensity also decreased by an additional factor of 2 between 100 and 130 eV. Changes in electron-scattering lengths are also significant in this energy region and will have an effect on absolute spectral intensities.

(24) The small photoemission feature at lowest binding energy in the 100-eV spectrum is the result of ionization of the Si 2p peaks with second-order light.

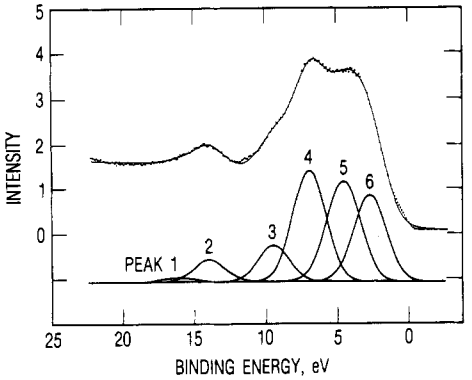

Figure 3. Fit of the 50-eV SiC valence band spectrum with six Voigt functions. The peak positions and widths are given in Table I.

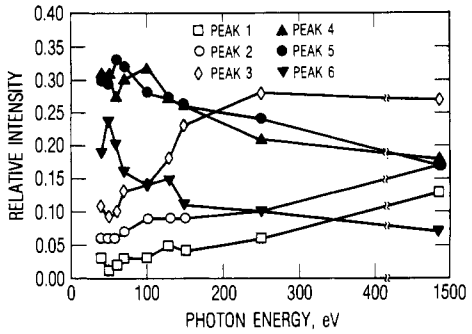

Figure 4. Relative intensities of SiC valence band peaks 1–6 as a function of photon energy obtained from data fits. The total spectral intensity at each photon energy is normalized to 1.

Table I. Binding Energy Positions and Widths of Peaks Used To Fit the 30–250-eV PES Data

peak	binding energy, eV	width, eV	peak	binding energy, eV	width, eV
1	16.10	1.60	4	7.05	1.70
2	14.00	1.60	5	4.65	1.75
3	9.50	1.60	6	2.80	1.70

character. The fitting program used has been described in detail elsewhere.[25] An additional peak, labeled 6, was needed at lowest binding energy to produce satisfactory fits. The peak locations, widths, and heights were allowed to vary in fitting the 50-eV spectrum. The resulting peak parameters are provided in Table I. Peak positions and widths were then constrained to these values in fitting the spectra obtained at the other photon energies. The peak widths were also allowed to vary in the 1486.6 eV data because of the lower resolution of the XPS spectrometer. The peaks in these spectral fits are not meant to represent ionizations from distinct valence band states but are used to map out intensity changes in the various regions of the valence band. The extended lattice nature of SiC should tend to disperse the energies of the valence band states through the Brillouin zone.

The relative, integrated peak intensities obtained from these fits are given in Figure 4, where the total spectral intensity at each photon energy has been normalized to 1. The 30 eV data are not included because the large, sloping background obscured peaks 1 and 2 and made fitting difficult. As expected from the qualitative description just given, peaks 1–3 rise with increasing photon energy, with peak 3 becoming the most intense feature at high photon energy. The relative intensity of peak 3 rises more rapidly than that of peaks 1 and 2 between 50 and 250 eV, nearly tripling, while the sum of the intensities of peaks 1 and 2 increases by only 80%. In the 50–250-eV photon energy region, C-based cross sections decline more rapidly than do Si levels (Figure 1), leading to the assignment of peaks 1 and 2 as being dominantly C 2s and peak 3 as being dominantly Si 3s. Figure 5 is a similar relative

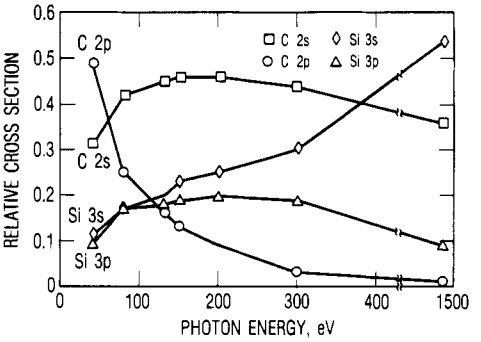

Figure 5. Theoretical photoionization cross sections of the important atomic valence levels in SiC as a function of photon energy. The cross sections are normalized as in Figure 4.

intensity plot for the theoretical atomic cross sections.[16] This figure indicates that the relative atomic Si 3s cross section nearly triples from 40 to 300 eV, while the C 2s level increases by approximately 50%, lending further support to the assignments of peaks 1–3.

Peaks 4–6 are the more intense features at low photon energy and exhibit large decreases in relative intensity with increasing photon energy, as demonstrated in Figure 4. This cross-sectional behavior mirrors that expected for C 2p atomic levels in Figures 1 and 5, leading to the assignment of these features as ionization from dominantly C 2p based levels. Note that the Si 3p cross section rises slowly from 50 to 150 eV in Figure 5 (similar to the Si 3s cross section), which eliminates the Si 3p level as being the major contributor to peaks 4–6.

The peak intensities in Figure 4 do not quantitatively follow the expected atomic trends (Figure 5). In general, the experimental intensity changes are much less dramatic than the theoretical changes, an effect that can be attributed to covalent bonding. For example, at 1486.6 eV, the theoretical atomic cross section for the C 2p ionization is approximately 100 times smaller than that of the Si 3s level and 66 times smaller than that of the C 2s level. However, the low binding energy, C 2p based valence features—peaks 4–6—still have significant intensity at 1486.6 eV. Peaks 4 and 5 each contribute approximately 20% of the total spectral intensity at 1486.6 eV, and peak 6 contributes 7%. This behavior clearly indicates mixing of these levels with atomic levels having much larger photoionization cross sections. (Si 3s, Si 3p, and C 2s are all possibilities.) The lowest binding energy feature, peak 6, has nearly the same intensity as peaks 4 and 5 at 50 eV but declines rapidly with increasing photon energy and becomes the weakest feature at 1486.6 eV. This intensity profile shows this peak to have more C 2p character and thus less mixing than peaks 4 and 5. These results indicate that states at the top of the valence band contain mostly nonbonding carbon electrons.

Finally, despite the significant intensity changes leading to their assignments, peaks 1–3 all exhibit mixed behavior. The high photon energy intensity changes of peak 3 more closely resemble the C 2s behavior in Figure 5, while peaks 1 and 2 continue to increase in relative intensity with increasing photon energy, which is a trait of Si 3s ionization. This is particularly evident if the total C 2s intensity is taken as the sum of peaks 1 and 2, which is greater than the intensity of peak 3 at 1486.6 eV. The atomic cross sections predict the Si 3s feature to be approximately 50% larger than the C 2s peak at this energy. These trends could indicate a high degree of covalent mixing between the C 2s and Si 3s levels and possibly interactions with other levels as well.

Comparison to Molecular Orbital Calculations. Figure 6 presents the molecular orbital energy level diagram obtained from a discrete variational (DV)–Xα calculation for an Si_4C_4 cluster having C_{3v} symmetry, adapted from ref 17. The calculated wave functions and eigenvalue energies are provided in Table II. The atomic constitutents of the molecular orbitals in Table II were used to determine the atomic origins of the molecular orbitals indicated in the Figure 6 diagram. The calculated molecular orbital positions are compared to the 150-eV spectrum in Figure 7, where the highest binding energy $1a_1$ state has been aligned

(25) Lince, J. R.; Stewart, T. B.; Hills, M. M.; Fleischauer, P. D.; Yarmoff, J. A.; Taleb-Ibrahimi, A. *Surf. Sci.* **1989**, *210*, 387.

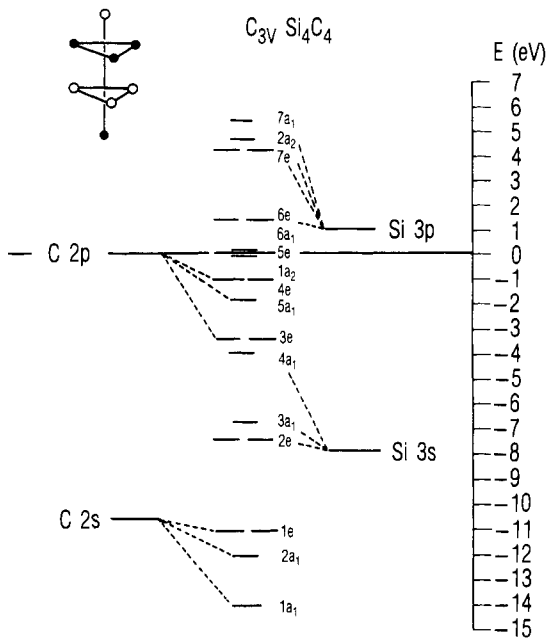

Figure 6. Energy level diagram for the C_{3v} Si_4C_4 cluster shown at the top of the figure. (Adapted from ref 17.)

Table II. Summary of the SiC Wave Functions for a C_{3v} Si_4C_4 Cluster (Adapted from Ref 17)[a]

		atomic orbital components			
MO	energy, eV	C 2s	C 2p	Si 3s	Si 3p
$7a_1$	5.34	3	11	21	64
$2a_2$	4.61		8		92
7e	4.23		8	1	92
6e	1.27		28	23	47
$6a_1$	0.00	3	29	29	34
empty levels					
full levels					
5e	0.00	1	89		10
$1a_2$	−0.10		92		8
4e	−1.10	1	89		10
$5a_1$	−1.95	7	66	15	12
3e	−3.44	1	64	3	32
$4a_1$	−4.04	16	72	7	5
$3a_1$	−6.83	8	37	46	8
2e	−7.49	48	5	42	6
1e	−11.04	66	5	23	7
$2a_1$	−12.04	69	3	22	6
$1a_1$	−13.97	69	1	25	6

[a] The squares of the molecular orbital wave function coefficients are given.

with the highest binding energy C 2s feature at 16.1 eV. The calculated energy level diagram agrees well qualitatively with the experimental peak assignments. The states under the peak 1–peak 2 regions are calculated to have predominantly C 2s character (66–69%), as was determined experimentally. The calculated highest occupied molecular orbitals (HOMO), 5e and $1a_2$, are approximately 90% C 2p and hence are essentially nonbonding, as anticipated from the intensity behavior of peak 6 just described.

The remaining levels at intermediate energies are predicted, for the most part, to be highly covalent. The states under peaks 4 and 5 are $4a_1$, 3e, $5a_1$, and 4e and are mostly C 2p (64–89%) but have significant amounts of Si character (10–35%). These results again agree qualitatively with the experiment, where peaks 4 and 5 were observed to have dominantly C 2p character but also retain more intensity at high photon energy than peak 6, indicative of a more highly mixed cross section. Finally, the $3a_1$ and 2e levels fall under peak 3, which was experimentally assigned as having mostly Si 3s atomic character. The calculation predicts these levels to be extremely covalent, containing a significant amount of Si 3s character (42–46%) in combination with 37% C 2p in the $3a_1$ and 48% C 2s in the 2e.

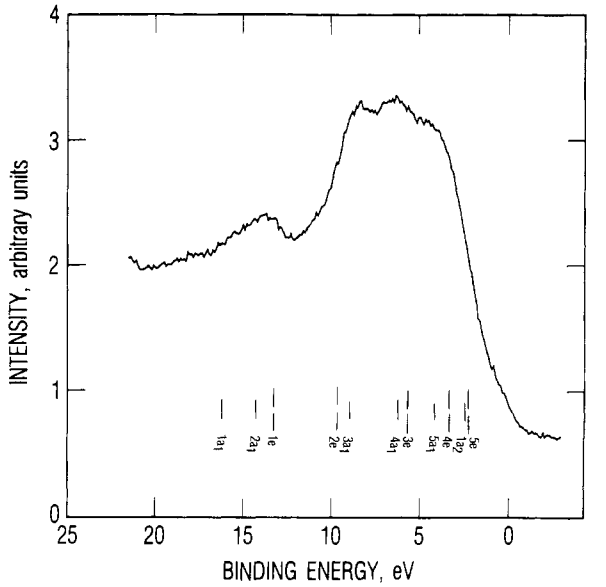

Figure 7. Comparison of the calculated occupied valence levels with the 150-eV valence band spectrum of α-SiC. The calculated levels are aligned with $1a_1$ at the highest binding energy SiC feature.

As demonstrated in Figure 7, the DV–Xα calculation does a fairly good job of predicting relative peak positions and splittings despite the extended lattice nature of the SiC sample and consequent energy dispersion of valence band states. In particular, the splitting of the C 2s peak into the $1a_1$ and $2a_1$ and 1e levels (which would be $1a_1$ and $1t_2$ in pure tetrahedral symmetry) is reproduced. The C 2s–Si 3s splitting is predicted to be approximately 4.5 eV, which is exactly the peak 2–peak 3 splitting determined from the peak fitting of the spectra (Table I). In general, the positions of the covalent C 2p features (peaks 4 and 5) and the essentially nonbonding levels of peak 6 are also accurately positioned. Finally, the calculation predicts the conduction band to be composed of primarily Si 3p based states, with large contributions from the Si 3s and C 2p atomic orbitals (Table II). We cannot experimentally determine the nature of the conduction band with PES. However, it is logical to predict that the lowest unoccupied levels will be dominantly Si 3p antibonding states if the valence band bonding levels are C 2p, based on a molecular orbital description. Note that the calculation fails in a very significant area, the splitting of the HOMO, the 5e, and the lowest unoccupied molecular orbital (LUMO), $6a_1$, which should correspond to the semiconductor's band gap. The calculation predicts these levels to overlap, making SiC a metal, a result that is obviously inconsistent with the known band gap of ~3 eV.

Theoretical spectra were generated from the Xα wave functions to determine if the wave functions accurately predict the amount of covalent mixing in SiC. To perform these calculations, the Gelius–Siegbahn model was used.[26] This model simply states that the ionization probability for a molecular orbital is the sum of the probabilities of its atomic components weighted by the squares of the appropriate molecular orbital wave function coefficients. Thus, a molecular orbital wave function of the form

$$\Psi = a\psi_{C\,2s} + b\psi_{C\,2p} + c\psi_{Si\,3s} + d\psi_{Si\,3p} \quad (1)$$

would have a PES intensity given by the following:

$$I = a^2\sigma_{C\,2s} + b^2\sigma_{C\,2p} + c^2\sigma_{Si\,3s} + d^2\sigma_{Si\,3p} \quad (2)$$

where σ_{nl} is the atomic subshell photoionization cross section.

Theoretical spectra were generated at photon energies of 40, 150, and 1486.6 eV by placing Gaussian peaks having fwhm = 2.5 eV at the appropriate calculated energies (corrected so that the $1a_1$ appears at 16.1 eV). A height determined from eq 2 was

(26) Gelius, U.; Siegbahn, K. *Faraday Discuss. Chem. Soc.* **1972**, No. 54, 257.

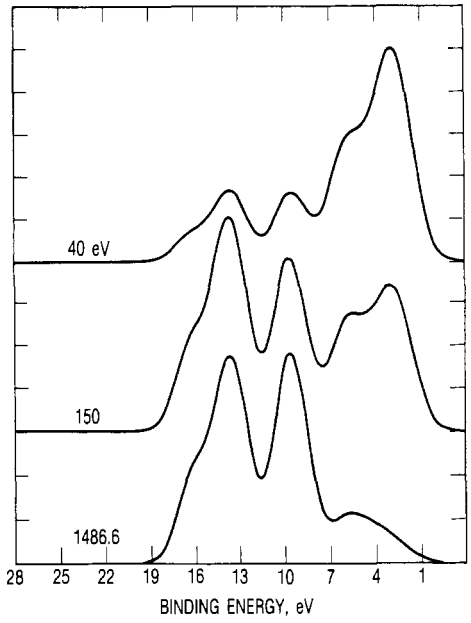

Figure 8. Theoretical valence band spectra at photon energies of (a) 40 eV, (b) 150 eV, and (c) 1486.6 eV. The spectra were made by using the Gelius–Siegbahn model with the wave functions in Table II and the cross sections adapted from ref 16.

used after accounting for electron occupation. These theoretical spectra are shown in Figure 8 and should be compared with the data obtained at comparable photon energies in Figure 2. The calculation gives a fairly accurate description of the general shape of the valence band at the three photon energies, but the relative peak intensities are not close to those observed experimentally, particularly at high photon energies. The general trend of decreasing intensity in the low binding energy region relative to the high binding energy regions is observed, but the changes in the theoretical spectra are much more dramatic than those observed experimentally. Also, the C 2s feature is calculated to be much more intense than the Si 3s peak at 150 eV; this is not observed experimentally, although the summed intensities of peaks 1 and 2 are greater than the intensity of peak 3 at 1486.6 eV. Finally, there is a gap between the Si 3s and the C 2p ionizations near 7 eV that is particularly evident in the 40- and 150-eV spectra predicted by the calculation. This gap is not seen in the experimental data.

The shortcomings of the theoretical spectra intensities are probably the result of inaccurate wave functions obtained from the Xα calculation. There is likely to be some error introduced by using atomic cross sections and the Gelius–Siegbahn model,[27] but these possibilities for error are outside the scope of this paper. It appears that the calculation predicts the C 2p features (peaks 4, 5, and possibly 6) to have too little mixing with other atomic orbitals. Although mixing with any other available atomic orbitals would increase the ionization cross section of the dominantly C 2p molecular orbitals, it is interesting to note that the calculation predicts very little C 2p–C 2s mixing or hybridization.

Tetrahedral C sites are often described as being sp^3 hybridized in the valence bond model, that is, as having four equivalent orbitals, each with 25% 2s and 75% 2p character. While this is obviously an overstatement of the extent of 2s–2p mixing, as evidenced by the well-characterized presence of a dominantly C 2s peak, the Xα calculation predicts only 1–5% C 2p character in the C 2s levels and only one C 2p level, the $4a_1$, with significant C 2s character (16%). If the C atom is viewed as purely the tetrahedral center of an isolated molecule, then in a strict molecular orbital interpretation of the electronic structure, the C 2s and 2p levels would reduce to states having a_1 and t_2 symmetry, respectively, and could not mix with each other. Mixing of the C 2s and 2p orbitals to form sp^3 hybrids (which can be expressed as linear combinations of these atomic orbitals) is consistent with molecular orbital theory, with both approaches resulting in the formation of molecular orbitals having a_1 and t_2 symmetry.[28] However, the experimental observation of a distinct, split C 2s based PES peak is not consistent with either of these views. The formation of sp^3-type σ orbitals with less than 25% mixing allows for the observation of distinct 2s and 2p PES peaks but still does not explain the C 2s splitting. The key to this phenomenon lies in the extended lattice nature of the solid. Because of this structure, C atoms (as well as Si atoms) act both as the center of tetrahedral sites and as ligands arranged in a tetrahedral array about a central atom. As a "ligand", the C 2s orbitals are split into a_1 and t_2 levels, which have the correct symmetry to mix with some of the C 2p orbitals, which transform as a_1, e, t_1, and 2 t_2's as T_d ligand group orbitals. This effect is observed in the C_{3v} Xα energy level diagram in Figure 6, where the C 2s levels are split into the $1a_1$, $2a_1$, and 1e levels ($1a_1$ and $1t_2$ in T_d symmetry). Therefore, C 2s–C 2p mixing is possible whether one examines the SiC system by using a simple valence bond approach, in a hybridized molecular orbital approach, or as an extended lattice system in a molecular orbital approach.[29]

Table III. Fitting Parameters and Relative Peak Intensities for Valence Band XPS of Single-Crystal and HP SiC

	single crystal			HP		
peak	energy, eV	width, eV	intensity	energy, eV	width, eV	intensity
1	16.1	3.8	0.13	16.1	4.3	0.07
2	14.3	2.7	0.17	14.0	3.8	0.18
3	9.8	2.2	0.28	9.5	2.6	0.32
4	7.4	2.7	0.18	7.1	2.5	0.16
5	5.0	2.6	0.17	4.7	2.5	0.16
6	3.1	2.3	0.07	2.5	3.2	0.10

If the amount of C 2s–C 2p mixing were increased in the calculated molecular orbitals, the intensity of the low binding energy features would increase relative to the C 2s and Si 3s peaks at higher binding energy in the theoretical spectrum at high photon energies. In addition, the C 2s intensity would decrease relative to the Si 3s peak at high photon energies because of the admixture of C 2p atomic character. Both of these changes to the theoretical spectra would bring them closer to the observed spectra at 150 and 1486.6 eV. The effects of greater C 2p–C 2s hybridization would not dramatically change the spectrum at 40 eV, because the C 2s and C 2p cross sections are both quite high at low photon energy relative to the Si 3s.

The low binding energy, C 2p based features could also gain intensity at high photon energies through greater covalent mixing with the Si 3s and 3p levels. Mixing with the Si 3p would certainly increase the intensity of the peak 4–peak 5 region, although not as greatly as the hybridization just discussed. The calculation predicts only 5–12% Si 3p character in the C 2p states (except for the 3e level). This amount seems quite low for a material thought to be highly covalent. On the other hand, any further mixing of the C 2p states with Si 3s levels would further decrease the intensity of the 3s feature at high photon energies, making it even weaker relative to the C 2s. It is quite likely, therefore, that a combination of more C 2s–C 2p hybridization and increased C 2p–Si 3p covalent mixing would result in a more accurate theoretical description of the electronic structure of α-SiC.

Comparison of Single-Crystal with Polycrystalline SiC. In Figure 9, the XPS valence band spectrum of the polycrystalline, hot-pressed SiC sample is compared to the single-crystal spectrum. It is evident that the spectra have essentially the same features. Hence, the polycrystalline sample can be described with a similar

(27) The Gelius–Siegbahn model is usually considered valid only at high photon energies (>200 eV) or when one constituent cross section is much greater than all other constituents.

(28) Cotton, F. A. *Chemical Applications of Group Theory*, 2nd ed.; Wiley-Interscience: New York, 1971; Chapter 8.

(29) It is interesting to note that the DV–Xα calculation predicts significant Si 3s–3p mixing, particularly in the conduction band states (see Table II).

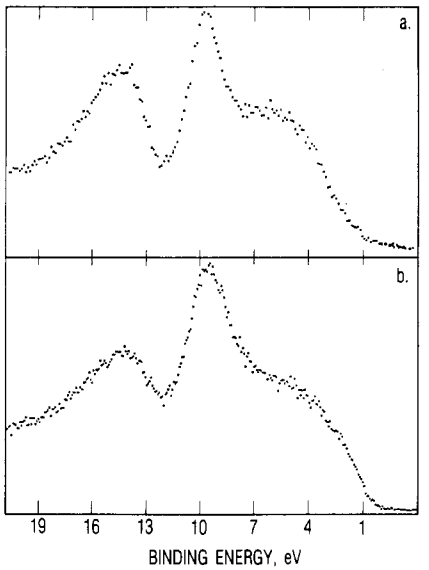

Figure 9. Comparison of the valence band spectra of (a) single-crystal α-SiC and (b) a polycrystalline, hot-pressed SiC coupon obtained at 1486.6 eV.

electronic structure as the single-crystal SiC. The parameters used to fit the valence bands of the two XPS spectra are given in Table III, where only the peak positions for the single crystal have been constrained. The polycrystalline spectrum (Figure 9) has broader features than the single-crystal spectrum; the peaks used to fit the polycrystalline spectrum are accordingly broader (Table III). In particular, the C 2s feature appears less intense and certainly broader for the polycrystalline sample, causing the Si 3s to gain in relative intensity compared to the single crystal. Also, the polycrystalline sample has more intensity at low binding energy, causing a larger peak 5–peak 6 splitting. These effects likely occur because of the presence of small crystals of several different polytypes in the HP sample. The polycrystalline sample, however, can likely be modeled by the single-crystal surface, because the electronic structures are basically the same.

Conclusions

Variable photon energy, valence band photoelectron spectroscopy of single-crystal α-SiC has revealed the electronic structure of the ceramic surface. The intensity changes in valence band features with changing incident photon energy have enabled us to determine the dominant, initial state atomic orbital contributions to different regions of the valence band. Specifically, the peaks at highest binding energy in the valence band (peaks 1 and 2 at 16.1 and 14.1 eV) have been shown to be predominantly C 2s in nature. Peak 3 at 9.6 eV exhibited cross-sectional behavior that identifies it as having significant Si 3s character. Finally, peaks 4–6, at low binding energies, were shown to be ionization from levels composed mostly of C 2p character. In addition, the effects of covalent bonding are observed in all of the features just described, as the intensity changes occurring with changing photon energy differed significantly from those predicted by the theoretical atomic photoionization cross sections. Specifically, C 2s–Si 3s covalency is indicated, and mixing of other atomic states into the dominantly C 2p peaks 4 and 5 is required to explain the high intensity of these features at high photon energies. Conversely, ionization from the top of the valence band (peak 6) revealed purer C 2p behavior, indicating little mixing, which is characteristic of essentially nonbonding levels. This result is in disagreement with band structure calculations for β-SiC, which predicted dominantly Si 3p character at the top edge of the valence band.[15]

These experimental assignments were further substantiated by comparison with a DV–Xα molecular orbital calculation. According to this calculation, states having essentially the same assignments as discussed in the previous paragraph were located in the same regions as the peaks in the spectra. The agreement between the experimental results and theory shows that the calculation on the small Si_4C_4 cluster produces molecular orbitals that accurately reflect the valence band electronic structure of the extended lattice wurtzite SiC sample. It is also significant that the ground state calculation accurately reflects the experimental spectrum without taking relaxation into account. Thus, it is likely that little change in the initial state wave functions occurs on ionization, indicating that the Si and C atoms have similar relaxation properties. Relaxation effects could contribute to the differing experimental and theoretical spectral intensities but must be examined through more extensive calculations. If relaxation effects are negligible, then the inaccurate theoretical peak intensities indicate that the calculation predicts too little covalent mixing in the molecular orbitals. In addition, the calculation likely underestimates the amount of C 2s–C 2p hybridization present in the sample. Correcting for this underestimation would also improve the theoretical spectra.

There are regions in the valence band that have PES intensity where the calculation predicts little intensity to exist, particularly between the Si 3s and C 2p features near 7 eV. This discrepancy could be the result of approximating the extended lattice electronic structure with molecular orbitals and thereby not accounting for the formation of bands. The bands would tend to spread the energy range over which occupied states are found in the valence band region and thus would spread PES intensity. Finally, the valence band electronic sturcture of a polycrystalline SiC sample was observed to be essentially the same as single-crystal α-SiC, with some broadening.

The ramifications of the electronic structure on the bonding and reactivity of SiC surfaces are manifold. The fact that the majority of the valence band electron density occurs in C 2p based features as opposed to Si 3p based features is consistent with the "carbidic" nature of the solid. These effects are also observed in the C and Si core level XPS shifts relative to the elemental species. The C 1s peak shifts to lower binding energy by approximately 1.3 eV, and the Si 2p peaks shift to higher binding energy by approximately 1.2 eV, consistent with greater valence electron density on the carbon atom.

The difference in electron density could also affect the bonding and reactivity of chemically different SiC surfaces. With the highest occupied energy levels having mostly C 2p character, an electron-withdrawing adsorbate would likely prefer adsorption on an electron-rich C atom. Furthermore, any loss of electrons or oxidation of the surface would be more likely to initiate at a carbon site than at an electron-deficient Si atom. Alternatively, the electron-deficient Si atom would likely interact more strongly with electron-donating adsorbates and similarly would be the preferred site for surface reduction reactions. There is evidence for differing reactivity of the α-SiC (000$\bar{1}$) and (0001), which ideally contain only C or Si atoms, respectively.[30] The C-containing surface has been shown to oxidize more readily than the Si surface, a finding that is consistent with this work. This reactivity difference is particularly evident in the initial uptake of oxygen, which is significantly higher on the (000$\bar{1}$) surface, perhaps showing that the C sites have a greater affinity for oxygen. We are currently studying the adsorption and reaction of SiC surfaces with a variety of electron-donating and -accepting species to determine if an observable distinction exists between electron donor and electron acceptor surface sites.

Acknowledgment. This work was supported by the Defense Advanced Research Projects Agency through the U.S. Air Force Systems Command, Space Systems Division Contract No. F04701-88-C-0089. Beam time was provided by the National Synchrotron Light Source, Brookhaven National Laboratory, which is supported by the U.S. Department of Energy, Division of Materials Sciences and Division of Chemical Sciences, under Contract No. DE-AC02-76CH00016.

(30) Muehlhoff, L.; Bozack, M. J.; Choyke, W. J.; Yates, J. T., Jr. *J. Appl. Phys.* **1986**, *60*, 2558.